First-principles predictions of temperature-dependent infrared dielectric function of polar materials by including four-phonon scattering and phonon frequency shift

Zhen Tong, Xiaolong Yang, Tianli Feng, Hua Bao, and Xiulin Ruan

Phys. Rev. B **101**, 125416 — Published 16 March 2020

DOI: 10.1103/PhysRevB.101.125416

First-principles predictions of temperature-dependent infrared dielectric function of polar materials by including four-phonon scattering and phonon frequency shift

Zhen Tong,[1,2] Xiaolong Yang,[3] Tianli Feng,[4] Hua Bao,[2,*] and Xiulin Ruan[1,†]

[1]*School of Mechanical Engineering and the Birck Nanotechnology Center, Purdue University, West Lafayette, Indiana 47907-2088, USA*

[2]*University of Michigan-Shanghai Jiao Tong University Joint Institute, Shanghai Jiao Tong University, Shanghai 200240, P. R. China.*

[3]*Institute for Advanced Study, Shenzhen University, Nanhai Avenue 3688, Shenzhen 518060, China.*

[4]*Materials Science and Technology Division, Oak Ridge National Laboratory, Oak Ridge,Tennessee 37831, USA*

Abstract

Recently, first-principles calculations based on density functional theory have been widely used to predict the temperature-dependent infrared spectrum of polar materials, but the calculations are usually limited to the harmonic frequency (0 K) and three-phonon scattering damping for the zone-center infrared-active optical phonon modes, and fail to predict the high-temperature infrared optical properties of materials such as sapphire (α-Al_2O_3), GaAs, TiO_2, etc. due to the neglect of high-order phonon scattering damping and phonon frequency shift. In this work, we implemented the first-principles calculations to predict the temperature-dependent infrared dielectric function of polar materials by including four-phonon scattering and phonon frequency shift. The temperature-dependent phonon damping by including three- and four-phonon scattering as well as the phonon frequency shift by including cubic, quartic anharmonicity and thermal expansion effect are calculated based on anharmonic lattice dynamics method. The infrared dielectric function of α-Al_2O_3 is parameterized and then the temperature-dependent infrared optical reflectance is determined. We find that our predictions agree better with the experimental data as compared to the previous density functional theory-based methods. This work will help to effectively predict the thermal radiative properties of polar materials at elevated temperature which is generally difficult to measure, and will enable predictive design of new materials for radiative applications.

PACS numbers:

I. INTRODUCTION

Infrared (IR) optical property has many important applications such as infrared detector, radiative cooling, radiative heat transfer, thermal light-emitting sources, and has attracted many research interests [1–10], particularly, many works [11–14] have concerned the temperature-dependent optical property due to high temperature applications. Recently, the density functional theory-based (DFT-based) first-principles method has been extensively used to predict the temperature-dependent infrared dielectric spectrum of polar materials. However, only the harmonic frequency (0 K) and three-phonon scattering damping were considered for the zone-center IR-active optical phonon modes among these predictions, which results in underestimated damping [15, 16] and unshifted frequency [7, 9, 14] as compared to experimental data at finite temperature. To overcome these limitations, extensive theoretical works [17–20] of calculating the temperature-dependent frequency shift and linewidth were conducted and the formulas were given, however, their applications are limited to the experimental fitting formulas [17, 18] or simple models [19, 20]. On the other hand, the *ab-initio* molecular dynamics (AIMD) approach [5] has been used to predict the IR optical properties of polar materials, which has the ability of including higher-order anharmonic effects on the optical phonon damping and frequency. However, AIMD still did not improve the results probably due to the simulation domain size effect in MD, which is limited by computational cost. Furthermore, Yang et al. [10] improved the DFT-based first-principles methods to investigate the infrared optical properties of polar materials, in which the four-phonon scattering based on the Feng-Ruan four-phonon scattering formalism [21] was included into the phonon damping. Their predictions agree well with experimental values after including the four-phonon scattering damping at high temperature for quite harmonic materials (BAs, cubic-SiC, α-SiO_2). However, for materials such as α-Al_2O_3, GaAs, TiO_2, etc., the neglect of phonon frequency shift may still lead to significant inaccuracy. In recent, Fugallo and Rousseau [22] predicted the temperature-dependent optical properties of MgO by considering the frequency shift and four-phonon damping of the zone-center optical phonon mode based on the density functional perturbation theory (DFPT) "$2n$+1" approach, in which the frequency-dependent phonon damping was predicted. On the other hand, some recent works have considered both four-phonon scattering and phonon frequency shift in thermal conductivity prediction [23, 24] with the quartic anharmonic force constants for arbitrary

q-points in Brillouin zone, but it has not been employed for zone-center IR modes and thermal radiative properties yet. Therefore, a fully first-principles calculations are necessary to be conducted to obtain the four-phonon linewidth and quartic anharmonic frequency shift of arbitrary **q**-points in the Brillouin zone and then capture the temperature-dependent features of the optical phonon frequency and damping for predicting the IR spectrum of polar materials.

In addition to numerical simulations, extensive experimental measurements have been widely carried out to obtain the finite temperature optical properties of polar materials using different techniques such as double-pass Perkin Elmer spectrometer[1], Fourier Transform Infrared (FTIR) spectrometer [25], ellipsometry[26], etc. However, these measurements are hard to perform at high temperature (over 1000 K) due to the limitation of self-radiation and thermal oxidation [26]. Also, it is difficult to separate temperature-dependent factor including three-, four-phonon or even higher order scattering as well as phonon frequency shift based on these directly experimental measurements.

In this work, we will investigate a comprehensive DFT-based first-principles calculations to predict the temperature-dependent IR optical properties of polar materials by including the four-phonon scattering and phonon frequency shift. In the calculation of optical phonon damping, the second-, third- and fourth-order interatomic force constants (2nd-, 3rd- and 4th-IFCs) are computed by using finite difference methods based on first-principles calculations for the determination of the three- and four-phonon scattering damping. For the calculations of temperature-dependent phonon frequency, the 3rd-, 4th-IFCs and thermal expansion coefficient are calculated to capture the frequency shift stemming from cubic (three-phonon scattering), quartic (four-phonon scattering) anharmonicity and thermal expansion. Finally, the calculated temperature-dependent IR optical phonon frequency and damping are used to parameterize the dielectric function and then predict the IR optical properties. The α-Al_2O_3 is used as an example material in the present work.

II. METHODOLOGY AND SIMULATION DETAILS

The dielectric function model used for describing the dielectric properties of α-Al_2O_3 can be written as the form [27–29]

$$\epsilon(\omega) = \epsilon_\infty \prod_j \frac{\omega_{j,\mathrm{LO}}^2 - \omega^2 + \mathrm{i}\gamma_{j,\mathrm{LO}}\omega}{\omega_{j,\mathrm{TO}}^2 - \omega^2 + \mathrm{i}\gamma_{j,\mathrm{TO}}\omega}, \tag{1}$$

where ϵ_∞ is the high frequency dielectric constant, ω_j is the resonance frequency, and LO and TO denote the longitudinal and transverse IR phonon modes, respectively. j goes over all the IR-active modes, and γ_j is the damping factor of the j-th resonance phonon mode.

From Eq. (1), the dielectric spectrum can be determined if the parameters (such as ω_j,γ_j) are known. Actually, the phonon frequency ω_j at finite temperature shifts away from their harmonic values due to anharmonicity and thermal expansion, which is not easy to be determined directly from theoretical methods. Also, the phonon damping factor γ, reciprocal of phonon lifetime (scattering rate), τ^{-1}, is hard to be obtained from theoretical calculations, and is usually fitted from the experimentally measured reflectance [28] or extracted from measured Raman linewidths [30].

A. Phonon frequency shift

In general, at finite temperature, the frequency shift originating from anharmonicity (phonon scattering) is given by the real part of the self-energy [18]. In phonon frequency shift, the three-phonon scattering contributes to the second order with bubble diagram, while the four-phonon scattering contributes to the first order with loop diagram [17, 18, 31, 32]. The three- and four-phonon term in the frequency shift can be calculated by [18, 33]

$$\begin{aligned}\Delta\omega_\lambda^{\mathrm{3ph}} =&\frac{\hbar}{16N_{\mathbf{q}}\omega_\lambda}\sum_{\lambda_1\lambda_2}\left[\left|V^{\mathrm{3ph}}_{\lambda-\lambda_1-\lambda_2}\right|^2\delta_{\mathbf{q}-\mathbf{q_1}-\mathbf{q_2}}\cdot\frac{n_1+n_2+1}{\omega_1\omega_2(\omega_\lambda-\omega_1-\omega_2)_P}+\right.\\ &\left.2\left|V^{\mathrm{3ph}}_{\lambda-\lambda_1-\lambda_2}\right|^2\delta_{\mathbf{q}+\mathbf{q_1}-\mathbf{q_2}}\cdot\frac{n_1-n_2}{\omega_1\omega_2(\omega_\lambda+\omega_1-\omega_2)_P}\right]\end{aligned} \tag{2}$$

$$\Delta\omega_\lambda^{\mathrm{4ph}} = \frac{\hbar}{8N_{\mathbf{q}}\omega_\lambda}\sum_{\lambda_1}V^{\mathrm{4ph}}_{-\lambda\lambda\lambda_1-\lambda_1}\cdot\frac{2n_1+1}{\omega_1} \tag{3}$$

where $\hbar$ is the reduced Planck constant, $N_{\mathbf{q}}$ is the number of $\mathbf{q}$-points in the Brillouin zone, ω is the frequency and $n=(e^{\hbar\omega/k_BT}-1)^{-1}$ is the phonon occupation number. $V^{\mathrm{3ph}}_{\pm}$ and $V^{\mathrm{4ph}}_{\pm\pm}$ are the three- and four-phonon scattering matrices given by [21]

$$V^{\mathrm{3ph}}_{\lambda\lambda_1\lambda_2} = \sum_{b,l_1b_1,l_2b_2}\sum_{\alpha\alpha_1\alpha_2}\Psi^{\alpha\alpha_1\alpha_2}_{0b,l_1b_1,l_2b_2}\frac{e^{\lambda}_{\alpha b}e^{\lambda_1}_{\alpha_1 b_1}e^{\lambda_2}_{\alpha_2 b_2}}{\sqrt{\bar{m}_b\bar{m}_{b_1}\bar{m}_{b_2}}}e^{i(\mathbf{k_1}\cdot\mathbf{r}_{l_1}+\mathbf{k_2}\cdot\mathbf{r}_{l_2})}, \tag{4}$$

$$V^{\mathrm{4ph}}_{\lambda\lambda_1\lambda_2\lambda_3} = \sum_{b,l_1b_1,l_2b_2,l_3b_3}\sum_{\alpha\alpha_1\alpha_2\alpha_3}\Phi^{\alpha\alpha_1\alpha_2\alpha_3}_{0b,l_1b_1,l_2b_2,l_3b_3}\frac{e^{\lambda}_{\alpha b}e^{\lambda_1}_{\alpha_1 b_1}e^{\lambda_2}_{\alpha_2 b_2}e^{\lambda_3}_{\alpha_3 b_3}}{\sqrt{\bar{m}_b\bar{m}_{b_1}\bar{m}_{b_2}\bar{m}_{b_3}}}e^{i(\mathbf{k_1}\cdot\mathbf{r}_{l_1}+\mathbf{k_2}\cdot\mathbf{r}_{l_2}+\mathbf{k_3}\cdot\mathbf{r}_{l_3})}, \tag{5}$$

where l, b, and α denote the indexes of unit cells, basis atoms, and (x,y,z) directions, respectively. $\mathbf{r}_l$ is the position of the primitive cell l, m is the mass of atom, e is the phonon eigenvector, Ψ and Φ are the 3rd- and 4th-IFCs.

On the other hand, the effect of thermal expansion may be taken into account by considering ω_λ^0 as the quasiharmonic frequency $\omega_\lambda^{\text{quasi}}$, in which the temperature-dependent lattice constant or thermal expansion are included. Thus the temperature-dependent frequency shift due to thermal expansion is given by [33, 34]

$$\Delta\omega_\lambda^{\text{quasi}} = \omega_\lambda^{\text{quasi}} - \omega_\lambda^0 = \omega_\lambda^0 \left\{ \exp\left[\int_0^T \alpha_V(T)dT\right]^{-g_\lambda} - 1 \right\}. \tag{6}$$

The α_V is the temperature-dependent thermal expansion coefficient given by

$$\alpha_V(T) = -\frac{k_B}{N_{\mathbf{q}}VB}\sum_\lambda g_\lambda \cdot \left(\frac{x}{2}\right) \cdot \left[1 - \coth^2\left(\frac{x}{2}\right)\right] \tag{7}$$

where V is the volume of the primitive, k_B is the Boltzmann constant and $x = \hbar\omega/k_BT$. The $g_\lambda = -\frac{V}{\omega_\lambda^0}\frac{\partial\omega_\lambda^0}{\partial V}$ is the Grüneisen parameter and $B = -V\frac{dP}{dV}$ is the bulk modulus.

Finally, the temperature-dependent phonon frequency of a certain phonon mode λ can be obtained as

$$\omega_\lambda(T) = \omega_\lambda^0 + \Delta\omega_\lambda^{3\text{ph}} + \Delta\omega_\lambda^{4\text{ph}} + \Delta\omega_\lambda^{\text{quasi}}. \tag{8}$$

B. Phonon damping with three and four phonon scattering

In general, the phonon damping γ (or scattering rate τ^{-1}) can be calculated through the anharmonic lattice method, in which the harmonic and anharmonic interatomic force constants are determined from first-principles calculations [9]. Here, both three- and four-phonon scattering are included into the phonon damping calculations. Based on Fermi's golden rule (FGR)[35], the $\gamma_\lambda^{3\text{ph}}$ due to three-phonon scattering rate $\tau_{3\text{ph},\lambda}^{-1}$, can be calculated by the summations of the probabilities of all possible three-phonon scattering events with single mode relaxation time approximation (SMRTA) [18, 35]

$$\gamma_\lambda^{3\text{ph}} = \tau_{3\text{ph},\lambda}^{-1} = \left(\sum_{\lambda_1\lambda_2}\Gamma_{\lambda\lambda_1}^{\lambda_2} + \frac{1}{2}\sum_{\lambda_1\lambda_2}\Gamma_\lambda^{\lambda_1\lambda_2}\right), \tag{9}$$

where λ_1 and λ_2 denote the second and third phonon mode that scatter with phonon mode λ. $\Gamma_{\lambda\lambda_1}^{\lambda_2}$ and $\Gamma_\lambda^{\lambda_1\lambda_2}$ represent the intrinsic three-phonon scattering rates for absorption processes $\lambda + \lambda_1 \to \lambda_2$ and emission processes $\lambda \to \lambda_1 + \lambda_2$, respectively.

Similarly, the $\gamma_\lambda^{4\text{ph}}$ due to four-phonon scattering rate $\tau_{4\text{ph},\lambda}^{-1}$ including all possible four-phonon interaction events can be obtained based on SMRTA [10, 18, 21, 33],

$$\gamma_\lambda^{4\text{ph}} = \tau_{4\text{ph},\lambda}^{-1} = \left(\frac{1}{6}\sum_{\lambda_1\lambda_2\lambda_3}\Gamma_\lambda^{\lambda_1\lambda_2\lambda_3} + \frac{1}{2}\sum_{\lambda_1\lambda_2\lambda_3}\Gamma_{\lambda\lambda_1}^{\lambda_2\lambda_3} + \frac{1}{2}\sum_{\lambda_1\lambda_2\lambda_3}\Gamma_{\lambda\lambda_1\lambda_2}^{\lambda_3}\right). \tag{10}$$

Finally, the phonon damping γ_λ of phonon mode λ can be obtained by including both three- and four-phonon scattering rate based on SMRTA,

$$\gamma_\lambda^{3+4\mathrm{ph}} = \frac{1}{\tau_\lambda^{3+4\mathrm{ph}}} = \tau_{3\mathrm{ph},\lambda}^{-1} + \tau_{4\mathrm{ph},\lambda}^{-1}. \tag{11}$$

From the above derivations, all the parameters in Eq. (1) will be determined if the 2nd-, 3rd-, and 4th-IFCs are provided. Here, the IFCs of α-Al_2O_3 were predicted from first-principles calculations, which were carried out in VASP [36]. The local-density approximation (LDA) [37] with the projector-augmented-wave method [38] was used for exchange and correlation functionals. The plane-wave energy cutoff is 520 eV, the energy convergence threshold is set for 10^{-8} eV and the electron $\mathbf{k}$ mesh is set as $3 \times 3 \times 3$. The lattice structure of α-Al_2O_3 belongs to the trigonal system (space group $R\overline{3c}$), which has rhombohedral primitive unit cell containing 2 formula units (10 atoms) as shown in Fig. 1(a). The optimized lattice parameters are a=5.140 Å and α=55.35° (experimental values [14] are a=5.128 Å and α=55.28°). The 2nd-IFCs and harmonic phonon frequencies were extracted by using Phonopy [39] which was interfaced to VASP [36], in which $3 \times 3 \times 3$ primitive cell was used to perform the density functional perturbation (DFPT) calculations. The 3rd-IFCs were calculated by using the code of thirdorder.py from the package of ShengBTE [40] based on VASP, in which the supercell was taken as $3 \times 3 \times 3$ primitive cell and the cutoff radius was considered up to 4th nearest neighboring atoms. The 4th-IFCs were calculated by using the in-house code developed based on thirdorder.py [40], in which the 3rd nearest neighboring cutoff was considered using $3 \times 3 \times 3$ primitive cell. The $\mathbf{q}$-points of 18×18×18 were used for the integration of the Brillouin zone based on careful convergence calculations. The three-phonon scattering rate was calculated by using ShengBTE [40], while the four-phonon scattering rate was computed by using the in-house code [21]. Also, the frequency shift due to four-phonon scattering and thermal expansion was calculated by using our in-house code [33].

III. RESULTS AND DISCUSSIONS

A. Temperature-dependent phonon frequency

The α-Al_2O_3 has a hexagonal conventional unitcell crystal structure with a rhombohedral primitive unitcell as shown in Fig. 1 (a), which results in anisotropic feature itself. In general,

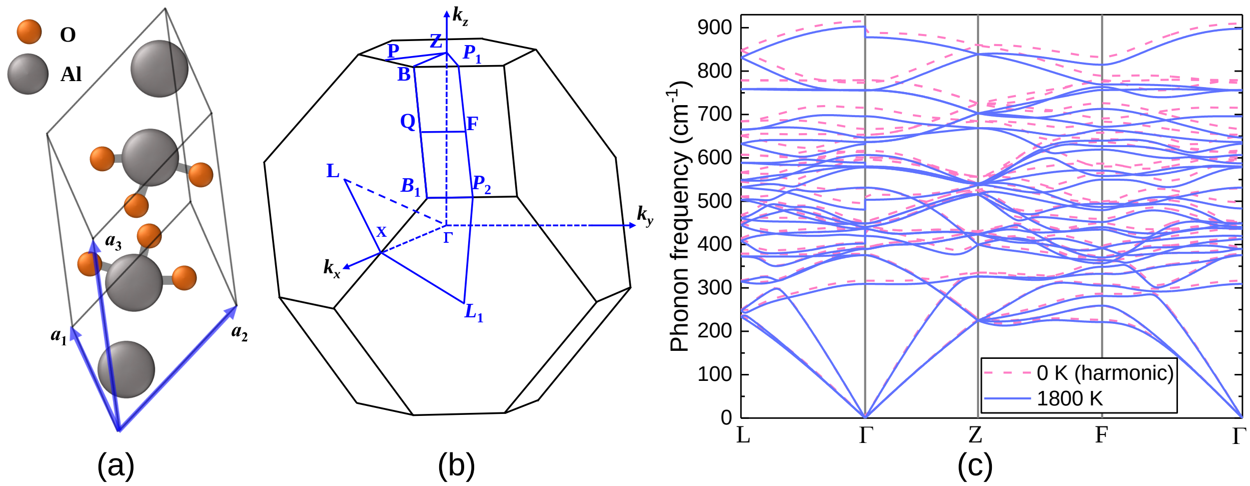

FIG. 1: (a) Crystal structure of primitive unitcell of α-Al_2O_3, which contains four aluminum atoms (gray color) and six oxygen atoms (orange color). The $\boldsymbol{a}_1$, $\boldsymbol{a}_2$ and $\boldsymbol{a}_3$ are the primitive lattice vectors. (b) First Brillouin zone of α-Al_2O_3. The high symmetry notations are referred to Ref. [41]. (c) Temperature-dependent phonon dispersion curve of α-Al_2O_3 calculated from first-principles. The harmonic frequency (dashed red line, at 0 K) corresponding to ω_λ^0 and the anharmonic frequency (solid blue line, at 1800 K) corresponding to $\omega_\lambda^0 + \Delta\omega_\lambda^{3ph} + \Delta\omega_\lambda^{4ph} + \Delta\omega_\lambda^{quasi}$ are shown for comparing the temperature effect.

the anisotropic dielectric of α-Al_2O_3 can be distinguished with ordinary ray spectrum (incident light with electric vector perpendicular to z-axis) and extraordinary ray spectrum (incident light with electric vector parallel to z-axis). It should be noted that there are multiple optical phonon modes in α-Al_2O_3, which are denoted as $2A_{1g}+2A_{1u}+3A_{2g}+2A_{2u}+4E_u+5E_g$ based on symmetry analysis [42, 43]. Among these modes, the A_{2u} (extraordinary ray) and E_u (ordinary ray) species are IR-active modes, A_{1g} and E_g are Raman-active modes, and A_{2g} and A_{1u} are spectroscopically inactive [43]. In addition, the frequency of TO and LO branches at zone center ($\mathbf{k} = 0$) of these IR-active modes depends on the direction in reciprocal space. For example, along the direction of $\Gamma \rightarrow \mathbf{X}$ (in xy plane) as shown in Fig. 1(b), the frequency is that of LO component of E_u or TO component of A_{2u}; along the direction of $\Gamma \rightarrow \mathbf{Z}$ (z-axis), the frequency is that of TO component of E_u or LO component of A_{2u}. Based on these theories, the TO and LO branch index of A_{2u} and E_u modes are determined using Phonopy [39].

Figure 1(c) shows the phonon dispersion spectrum along the high symmetry points in first Brillouin zone as denoted in Fig. 1(b) at 0 K and 1800 K , respectively. From Fig. 1(c), we can see that the phonon frequency decreases as temperature increases, which is mainly due to the positive Grüneisen parameters and thermal expansion coefficients in α-Al_2O_3. We can also see that the frequency shift in optical modes are significant, which is particularly important in determining the dielectric spectrum especially at elevated temperature. Moreover, this result indicates that the overall temperature effect on the vibrational frequencies can be successfully captured for the whole Brillouin zone based on our method.

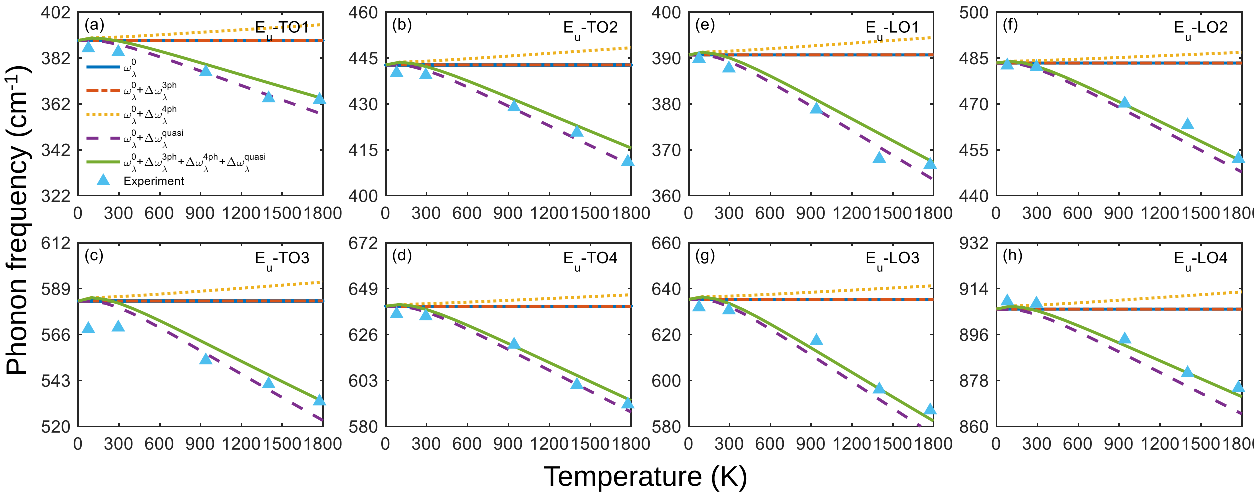

FIG. 2: The temperature-dependent phonon frequency calculated from first-principles are compared with experimental data. The IR-active optical mode with symmetry of E_u which includes 4 species in α-Al_2O_3 at Γ point are calculated in this work. The frequency shift effect on harmonic frequency (solid blue line denoted with ω_λ^0) due to three-phonon scattering (dot dash brown line denoted with $\omega_\lambda^0 + \Delta\omega_\lambda^{3ph}$), four-phonon scattering (dotted yellow line denoted with $\omega_\lambda^0 + \Delta\omega_\lambda^{4ph}$), thermal expansion (dashed purple line denoted with $\omega_\lambda^0 + \Delta\omega_\lambda^{quasi}$) and total effects (solid green line denoted with $\omega_\lambda^0 + \Delta\omega_\lambda^{3ph} + \Delta\omega_\lambda^{4ph} + \Delta\omega_\lambda^{quasi}$) are calculated for TO (a-d) and LO (e-h) modes. The experimental data [28] (upward-pointing triangle) fitted from the experimental measurements of reflectance of α-Al_2O_3 are shown for comparison.

On the other hand, the temperature-dependent reflectance spectrum for ordinary ray of α-Al_2O_3 have been experimentally determined in Piriou's work [44]. Based on these reflectance spectrum, the temperature-dependent phonon frequencies of the IR phonon modes were further fitted by using the dielectric model of Eq. 1 in Gervais's work [28]. Although they obtained the finite temperature IR phonon modes' frequencies, the thermal expansion and purely anharmonic effects in the observed frequency shifts were not possible to be separately identified as claimed in their work [28]. However, in our work, the frequency shifts due to thermal expansion and quartic anharmonicity effects are separately calculated from first-principles calculations.

Finally, the temperature-dependent phonon frequencies of E_u species IR-active modes calculated using our method based on first-principles calculations are compared with the experimental fitting data in Ref. [28], which are shown in Fig. 2. We can see that our calculated temperature-dependent phonon frequencies ($\omega_\lambda^0 + \Delta\omega_\lambda^{3ph} + \Delta\omega_\lambda^{4ph} + \Delta\omega_\lambda^{quasi}$) agree well with the experimental data in general. Actually, it can be found that our predictions are underestimated as compared to experimental values, which might be improved if the higher-order (higher than fourth-order) anharmonic frequency shift are included. It can also be seen that the frequency shifts are negative due to thermal expansion ($\Delta\omega_\lambda^{quasi}$) while are positive due to four-phonon anharmonicity ($\Delta\omega_\lambda^{4ph}$). Also, it should be noted that the four-phonon anharmonicity makes the major contribution to the frequency shift and it is generally much larger than that of three-phonon anharmonicity, which is similar to the conclusion in Ref. [32, 33]. Moreover, the magnitude of $\Delta\omega_\lambda^{quasi}$ is larger than that of $\Delta\omega_\lambda^{4ph}$, which indicates that the thermal expansion is the predominant effect on the frequency shift and this predominance finally results in the negative total frequency shift. The softening frequencies of these phonon modes are mainly due to the positive Grüneisen parameters and thermal expansion coefficients in α-Al_2O_3. In addition, the magnitude of the frequency shift increases with increasing temperature, which indicates the temperature effect on vibrational frequencies is significant especially at elevated temperature.

B. Temperature-dependent phonon damping

The temperature-dependent three-phonon (γ_λ^{3ph}) and four-phonon (γ_λ^{4ph}) scattering damping of the IR-active phonon modes in α-Al_2O_3 are shown in Fig. 3, respectively. We can see that γ_λ^{3ph} dominates at low to intermediate temperatures, but the γ_λ^{4ph} can become non-negligible or even comparable with γ_λ^{3ph} for some modes at high temperature (∼1800 K), which indicates that the four-phonon scattering contribution to the phonon damping is significant due to the strong anharmonic phonon-phonon scattering at elevated temperature. On the other hand, we can see that the phonon damping scales with temperature as $\gamma_\lambda^{3ph} \sim T$

and $\gamma_\lambda^{4ph} \sim T^2$. Hence we can write the total phonon damping $\gamma = A + BT + CT^2 + ...$, in which the coefficients of A, B and C are related to isotope, three-, and four-phonon scattering, respectively. This formula is very useful to understand different damping mechanisms in the total damping factor obtained through experiments or modeling (such as molecular dynamics).

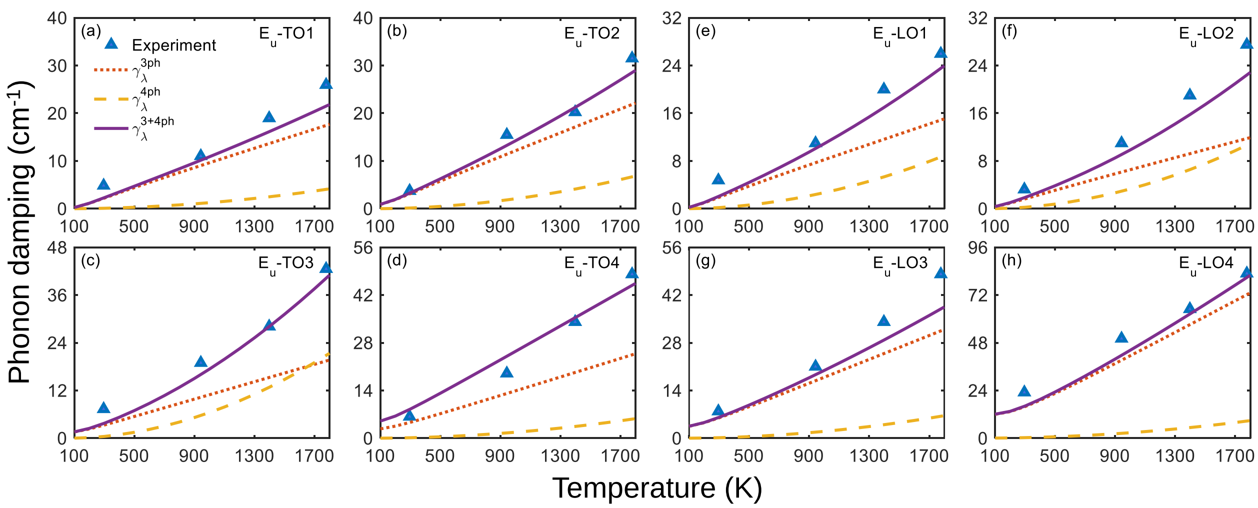

FIG. 3: The temperature-dependent phonon damping γ calculated from first-principles are compared with experimental data. The γ of IR-active optical mode with symmetry of E_u which includes 4 species in α-Al_2O_3 at Γ point are calculated in this work. The γ_λ^{3ph} (dotted red line) and γ_λ^{4ph} (dashed yellow line) due to three- and four-phonon scattering are shown as a function of temperature for TO (a-d) and LO (e-h) modes, respectively. The experimental data [28] (upward-pointing triangle) fitted from the experimental measurements of reflectance of α-Al_2O_3 are shown to compare with the calculated total phonon damping γ_λ^{3+4ph} (solid purple line).

C. Temperature-dependent reflectance spectrum

Similarly, the high frequency dielectric constant ϵ_∞ is calculated from first-principles calculations with the values of $\epsilon_\infty^\parallel = 3.21$ (ordinary ray) and $\epsilon_\infty^\perp = 3.20$ (extraordinary ray), which agree well with the experimental values of $\epsilon_\infty^\parallel = 3.2$ and $\epsilon_\infty^\perp = 3.1$ [2]. Finally, by submitting the obtained high frequency dielectric constant ϵ_∞, temperature-dependent phonon frequency ω_λ and damping γ_λ of the IR-active modes into the dielectric function of Eq. 1, the temperature-dependent dielectric spectrum is determined. Furthermore, the temperature-dependent semi-infinite normal incident reflectance R can be determined with the relation of $R = \left\{ \sqrt{\epsilon_1^2 + \epsilon_2^2} + 1 - \sqrt{2\left(\sqrt{\epsilon_1^2 + \epsilon_2^2} + \epsilon_1\right)} \right\} / \left\{ \sqrt{\epsilon_1^2 + \epsilon_2^2} + 1 + \sqrt{2\left(\sqrt{\epsilon_1^2 + \epsilon_2^2} + \epsilon_1\right)} \right\}$, in which ϵ_1 and ϵ_2 is the real and imaginary part of ϵ, respectively.

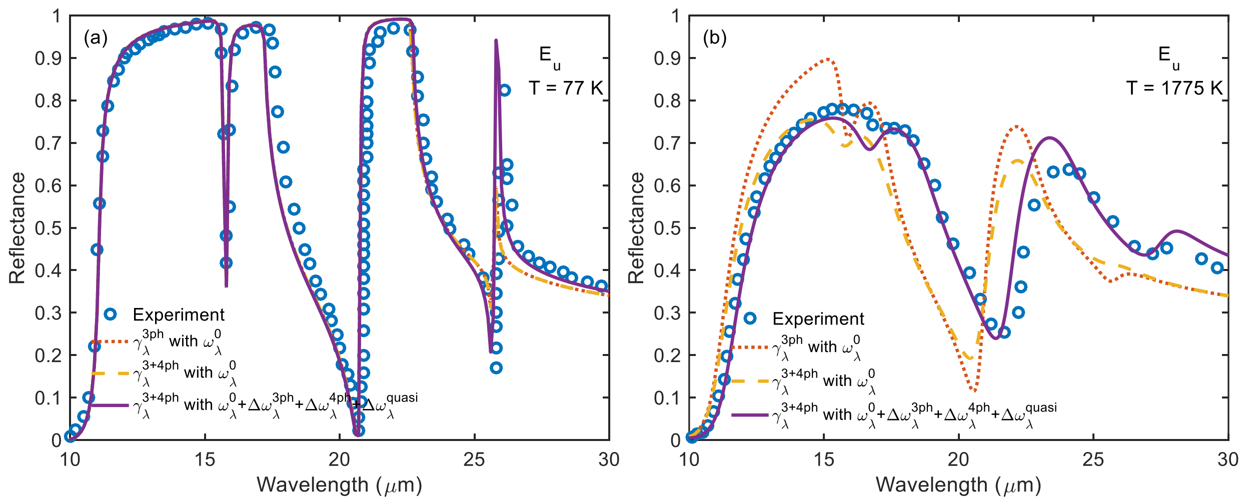

FIG. 4: The semi-infinite normal reflectance calculated from first-principles are compared with experimental data. The temperature-dependent reflectance spectrum (ordinary ray) of α-Al_2O_3 are shown: (a) at 77 K and (b) at 1775 K. The reflectance calculated using $\gamma_\lambda^{3\mathrm{ph}}$ with ω_λ^0 (dotted red line), $\gamma_\lambda^{3+4\mathrm{ph}}$ with ω_λ^0 (dashed yellow line), and $\gamma_\lambda^{3+4\mathrm{ph}}$ with $\omega_\lambda^0 + \Delta\omega_\lambda^{3\mathrm{ph}} + \Delta\omega_\lambda^{4\mathrm{ph}} + \Delta\omega_\lambda^{\mathrm{quasi}}$ (solid purple line) are plotted for comparison with experimental data [44] (blue circle).

The temperature-dependent reflectance spectrum (ordinary ray) of α-Al_2O_3 are shown in Fig. 4 at 77 K and 1775 K. At low temperature (77 K) in Fig. 4(a), it can be seen that the effect of frequency shift and four-phonon scattering damping on the reflectance is not significant. However, at high temperature (1775 K) in Fig. 4(b), the reflectance calculated using $\gamma_\lambda^{3+4\mathrm{ph}}$ with ω_λ^0 (dashed yellow line) reduces the reflectance peak compared to the curve using $\gamma_\lambda^{3\mathrm{ph}}$ with ω_λ^0 (dotted red line), but there still exists a peak shift deviated from the experimental data. Meanwhile, after including the frequency shift and plotting the reflectance using $\gamma_\lambda^{3+4\mathrm{ph}}$ with $\omega_\lambda^0 + \Delta\omega_\lambda^{3\mathrm{ph}} + \Delta\omega_\lambda^{4\mathrm{ph}} + \Delta\omega_\lambda^{\mathrm{quasi}}$, the reflectance spectrum denoted with dashed yellow line becomes the solid purple line as shown in Fig. 4(b), which results in excellent agreement with experimental data. This result indicates that the frequency shift is necessary to be included in the dielectric spectrum prediction at high temperature. Our method improved the previous methods which did not consider the phonon frequency shift thus resulting in the prediction inaccuracy of the optical properties for strongly anharmonic materials at high temperature.

On the other hand, the reflectance spectrum of extraordinary at room temperature is also calculated and it is compared with the experimental measurements [2], which is shown in Fig. 5. We can see that the calculated reflectance which includes the frequency shift and four-phonon scattering damping matches well overall with experimental data. All of these results give the confidence of our method with a comprehensive first-principles calculations of predicting the temperature-dependent IR dielectric function of polar materials by including the four-phonon scattering and phonon frequency shift.

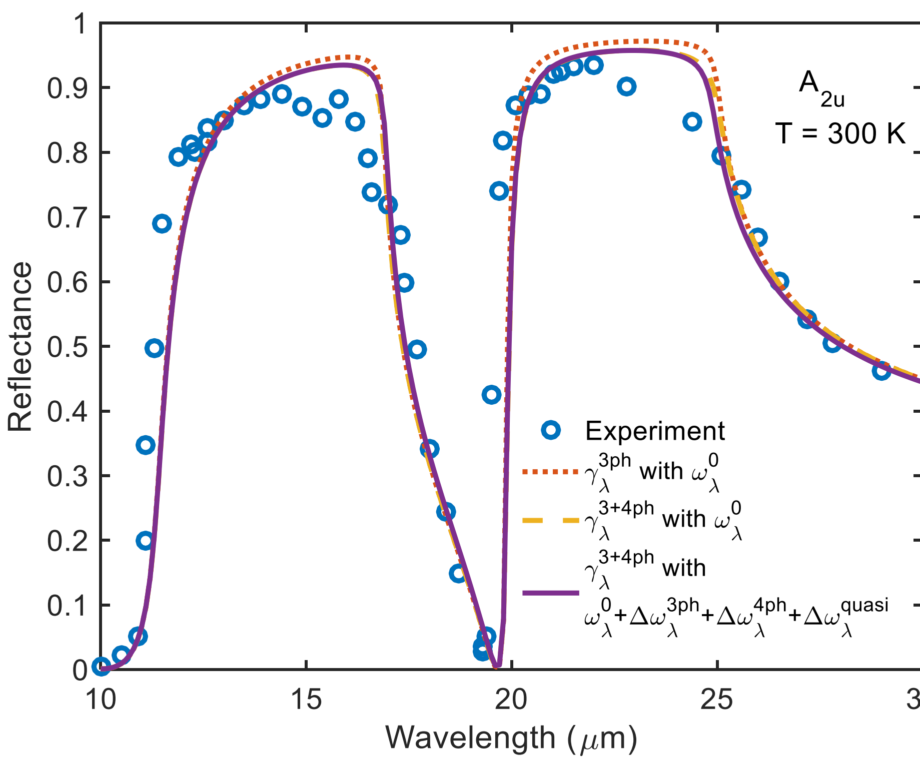

FIG. 5: The semi-infinite normal reflectance calculated from first-principles are compared with experimental data. The temperature-dependent reflectance spectrum (extraordinary ray) of α-Al_2O_3 are shown at 300 K. The reflectance calculated using γ_λ^{3ph} with ω_λ^0 (dotted red line), γ_λ^{3+4ph} with ω_λ^0 (dashed yellow line), and γ_λ^{3+4ph} with $\omega_\lambda^0 + \Delta\omega_\lambda^{3ph} + \Delta\omega_\lambda^{4ph} + \Delta\omega_\lambda^{quasi}$ (solid purple line) are plotted for comparison with experimental data [2] (blue circle).

CONCLUSIONS

In summary, by performing the DFT-based first-principles calculations, we predict the temperature-dependent IR dielectric function of polar materials by including the four-phonon scattering and phonon frequency shift. The α-Al_2O_3 is used as an example material in this work. The three- and four-phonon scattering effect on phonon damping as well as the cubic, quartic anharmonicity and thermal expansion effect on frequency shift are calculated based on anharmonic lattice method with perturbation theory to predict the temperature-dependent IR optical properties. Our predictions are in excellent agreement with the reported experimental data. Based on the analysis of the effect of three- and four-phonon scattering on the phonon damping separately, we find that the four-phonon scattering damping is comparable to three-phonon scattering damping at high temperature for some infrared phonon modes in α-Al_2O_3. We also find that the phonon frequency is softened due to thermal expansion and is hardened due to quartic anharmonicity, but the former dominates and final results in the total negative frequency shift in α-Al_2O_3. Using these obtained temperature-dependent infrared optical phonon properties to parameterize the infrared dielectric function, the predicted semi-infinite reflectance agrees better with the experimental values as compared to the previous DFT-based methods. This method paves the way for effectively modeling the temperature-dependent optical properties of polar materials which is generally not easy to obtain through experimental measurements especially at high temperatures. Therefore, it enables predictive design of new materials for radiative applications.

ACKNOWLEDGEMENTS

Simulations were preformed at the Rosen Center for Advanced Computing (RCAC) of Purdue University. X.R. acknowledges the partial support by the National Science Foundation (Award No. 1150948). H.B. acknowledges the support by the National Natural Science Foundation of China (Grant No. 51676121). Z.T. also thanks for the financial support of Chinese Scholarship Council (CSC, No. 201806230169).

* Electronic address: hua.bao@sjtu.edu.cn

† Electronic address: ruan@purdue.edu

[1] W. G. Spitzer, D. A. Kleinman, and C. J. Frosch, Physical Review **113**, 133 (1959), ISSN 0031-899X, URL https://link.aps.org/doi/10.1103/PhysRev.113.133.

[2] A. S. Barker, Physical Review **132**, 1474 (1963), ISSN 0031-899X, URL https://link.aps.org/doi/10.1103/PhysRev.132.1474.

[3] F. Gervais and B. Piriou, Physical Review B **11**, 3944 (1975), ISSN 0556-2805, URL https://link.aps.org/doi/10.1103/PhysRevB.11.3944.

[4] H. Bao and X. Ruan, International Journal of Heat and Mass Transfer **53**, 1308 (2010), ISSN 00179310, URL https://linkinghub.elsevier.com/retrieve/pii/S0017931009006930.

[5] H. Bao, B. Qiu, Y. Zhang, and X. Ruan, Journal of Quantitative Spectroscopy and Radiative Transfer **113**, 1683 (2012), ISSN 00224073, URL http://linkinghub.elsevier.com/retrieve/pii/S0022407312002336.

[6] J. Yang, M. Xu, and L. Liu, Journal of Quantitative Spectroscopy and Radiative Transfer **184**, 111 (2016), ISSN 00224073, URL https://linkinghub.elsevier.com/retrieve/pii/S0022407316301595.

[7] A. Mock, R. Korlacki, S. Knight, and M. Schubert, Physical Review B **95**, 165202 (2017), URL https://link.aps.org/doi/10.1103/PhysRevB.95.165202.

[8] G. Domingues, A. M. Monthe, S. Guvelou, and B. Rousseau, Journal of Quantitative Spectroscopy and Radiative Transfer **205**, 220 (2018), ISSN 00224073, URL https://linkinghub.elsevier.com/retrieve/pii/S0022407317303448.

[9] Z. Tong, L. Liu, L. Li, and H. Bao, Physica B: Condensed Matter **537**, 194 (2018), ISSN 09214526, URL http://linkinghub.elsevier.com/retrieve/pii/S092145261830142X.

[10] X. Yang, T. Feng, J. S. Kang, Y. Hu, J. Li, and X. Ruan, arXiv:1908.05121 [cond-mat] (2019), arXiv: 1908.05121, URL http://arxiv.org/abs/1908.05121.

[11] D. Olego and M. Cardona, Physical Review B **25**, 3889 (1982), ISSN 0163-1829, URL https://link.aps.org/doi/10.1103/PhysRevB.25.3889.

[12] S. Dakshinamurthy, N. R. Quick, and A. Kar, Journal of Physics D: Applied Physics **40**, 353 (2007), ISSN 0022-3727, 1361-6463, URL http://stacks.iop.org/0022-3727/40/i=2/a=010?key=crossref.3753475dc885e1a9b426efbe602f855d.

[13] K. M. Pitman, A. M. Hofmeister, A. B. Corman, and A. K. Speck, Astronomy & Astrophysics **483**, 661 (2008), ISSN 0004-6361, 1432-0746, URL http://www.aanda.org/10.1051/

0004-6361:20078468.

[14] J. Breeze, *Jonathan Breeze - Temperature and Frequency Dependence of Complex Permittivity in Metal Oxide Dielectrics: Theory, Modelling and Measurement* (Springer Theses, London South Bank University, London, 2016).

[15] A. Debernardi, S. Baroni, and E. Molinari, Physical Review Letters **75**, 1819 (1995), ISSN 0031-9007, 1079-7114, URL https://link.aps.org/doi/10.1103/PhysRevLett.75.1819.

[16] A. Debernardi, Physical Review B **57**, 12847 (1998), ISSN 0163-1829, 1095-3795, URL https://link.aps.org/doi/10.1103/PhysRevB.57.12847.

[17] M. Balkanski, R. F. Wallis, and E. Haro, Physical Review B **28**, 1928 (1983), ISSN 0163-1829, URL https://link.aps.org/doi/10.1103/PhysRevB.28.1928.

[18] A. A. Maradudin and A. E. Fein, Physical Review **128**, 2589 (1962), ISSN 0031-899X, URL https://link.aps.org/doi/10.1103/PhysRev.128.2589.

[19] M. R. Monga and K. N. Pathak, Physical Review B **18**, 5859 (1978), ISSN 0163-1829, URL https://link.aps.org/doi/10.1103/PhysRevB.18.5859.

[20] P. Procacci, G. Cardini, R. Righini, and S. Califano, Physical Review B **45**, 2113 (1992), ISSN 0163-1829, 1095-3795, URL https://link.aps.org/doi/10.1103/PhysRevB.45.2113.

[21] T. Feng and X. Ruan, Physical Review B **93**, 045202 (2016), URL https://link.aps.org/doi/10.1103/PhysRevB.93.045202.

[22] G. Fugallo, B. Rousseau, and M. Lazzeri, Physical Review B **98**, 184307 (2018), ISSN 2469-9950, 2469-9969, URL https://link.aps.org/doi/10.1103/PhysRevB.98.184307.

[23] N. K. Ravichandran and D. Broido, Physical Review B **98**, 085205 (2018), URL https://link.aps.org/doi/10.1103/PhysRevB.98.085205.

[24] Y. Xia, Applied Physics Letters **113**, 073901 (2018), ISSN 0003-6951, URL https://aip.scitation.org/doi/full/10.1063/1.5040887.

[25] P. R. Griffiths and J. A. D. Haseth, *Fourier Transform Infrared Spectrometry* (John Wiley & Sons, 2007), ISBN 978-0-470-10629-7.

[26] H. Fujiwara, *Spectroscopic Ellipsometry* (John Wiley & Sons Ltd, England, 2007), ISBN 4-621-07253-6.

[27] A. S. Barker, Physical Review **136**, A1290 (1964), ISSN 0031-899X, URL https://link.aps.org/doi/10.1103/PhysRev.136.A1290.

[28] F. Gervais and B. Piriou, Journal of Physics C: Solid State Physics **7**, 2374 (1974),

ISSN 0022-3719, URL http://stacks.iop.org/0022-3719/7/i=13/a=017?key=crossref.a70016f366b7e910c114a6eb49f3e0e2.

[29] D. W. Berreman and F. C. Unterwald, Physical Review **174**, 791 (1968), ISSN 0031-899X, URL https://link.aps.org/doi/10.1103/PhysRev.174.791.

[30] M. Ashkin, J. H. Parker, and D. W. Feldman, Solid State Communications **6**, 343 (1968), ISSN 0038-1098, URL http://www.sciencedirect.com/science/article/pii/003810986890152X.

[31] M. Lazzeri, M. Calandra, and F. Mauri, Physical Review B **68**, 220509 (2003), URL https://link.aps.org/doi/10.1103/PhysRevB.68.220509.

[32] T. Tadano and S. Tsuneyuki, Journal of the Physical Society of Japan **87**, 041015 (2018), ISSN 0031-9015, 1347-4073, URL http://journals.jps.jp/doi/10.7566/JPSJ.87.041015.

[33] T. Feng, X. Yang, and X. Ruan, Journal of Applied Physics **124**, 145101 (2018), ISSN 0021-8979, 1089-7550, URL http://aip.scitation.org/doi/10.1063/1.5048799.

[34] U. Argaman, E. Eidelstein, O. Levy, and G. Makov, Physical Review B **94**, 174305 (2016), URL https://link.aps.org/doi/10.1103/PhysRevB.94.174305.

[35] G. D. Mahan, *Many-Particle Physics* (Kluwer Academic/Plenum Publishers, New York, NY Boston Dordrecht London Moscow, 2000), 3rd ed., ISBN 0-306-46338-5.

[36] G. Kresse and J. Hafner, Physical Review B **47**, 558 (1993), ISSN 0163-1829, 1095-3795, URL https://link.aps.org/doi/10.1103/PhysRevB.47.558.

[37] L. Hedin and B. I. Lundqvist, Journal of Physics C: Solid State Physics **4**, 2064 (1971), ISSN 0022-3719, URL http://stacks.iop.org/0022-3719/4/i=14/a=022?key=crossref.334ee45c6e999b9902d2e8596d9cea51.

[38] G. Kresse and D. Joubert, Physical Review B **59**, 1758 (1999), ISSN 0163-1829, 1095-3795, URL https://link.aps.org/doi/10.1103/PhysRevB.59.1758.

[39] A. Togo and I. Tanaka, Scripta Materialia **108**, 1 (2015), ISSN 13596462, URL https://linkinghub.elsevier.com/retrieve/pii/S1359646215003127.

[40] W. Li, J. Carrete, N. A. Katcho, and N. Mingo, Computer Physics Communications **185**, 1747 (2014), ISSN 00104655, URL http://linkinghub.elsevier.com/retrieve/pii/S0010465514000484.

[41] W. Setyawan and S. Curtarolo, Computational Materials Science **49**, 299 (2010), ISSN 09270256, URL http://linkinghub.elsevier.com/retrieve/pii/S0927025610002697.

[42] S. P. S. Porto and R. S. Krishnan, The Journal of Chemical Physics **47**, 1009 (1967), ISSN 0021-9606, 1089-7690, URL http://aip.scitation.org/doi/10.1063/1.1711980.

[43] P. F. McMillan and N. L. Ross, Physics and Chemistry of Minerals **14**, 225 (1987).

[44] B. Piriou, Influ Temp Rev Hautes Temper Refract **3**, 109 (1966).